

**Estimating air–sea
heat fluxes and
ocean heat content
changes**

L. Cheng et al.

**Global representation of tropical
cyclone-induced ocean thermal changes
using Argo data – Part 2: Estimating
air–sea heat fluxes and ocean heat
content changes**

L. Cheng¹, J. Zhu¹, and R. L. Sriver²

¹International Center for Climate and Environment Sciences, Institute of Atmospheric Physics, Chinese Academy of Sciences, Beijing, China

²Department of Atmospheric Sciences, University of Illinois, Urbana-Champaign, IL, USA

Received: 30 October 2014 – Accepted: 28 November 2014 – Published: 12 December 2014

Correspondence to: J. Zhu (jzhu@mail.iap.ac.cn)

Published by Copernicus Publications on behalf of the European Geosciences Union.

Title Page

Abstract

Introduction

Conclusions

References

Tables

Figures



Back

Close

Full Screen / Esc

Printer-friendly Version

Interactive Discussion



Estimating air–sea heat fluxes and ocean heat content changes

L. Cheng et al.

Title Page

Abstract

Introduction

Conclusions

References

Tables

Figures

◀

▶

◀

▶

Back

Close

Full Screen / Esc

Printer-friendly Version

Interactive Discussion



temperature (i.e. TCs cause more cooling during warming seasons). On the contrary, subsurface OHC changes are not significant for weak storms compared to background variability. The authors attribute the lack of a subsurface response to a diminished role of entrainment in weaker TCs compared combined with enhanced air–sea heat fluxes and vertical advection. For strong storms, subsurface warming is generally consistent with mixed layer cooling (same magnitude and opposite sign).

In part I of this study, we present a new technique using ARGO data that utilizes a method aggregating global TC-induced ocean thermal responses into a Langragian footprint coordinate system. In brief, the footprint is created as a function of horizontal distance across the track (perpendicular to the storm’s direction of motion), water depth, and elapsed time after the TC passed. We separate TCs into two categories: tropical storm/tropical depression (TS/TD) and hurricanes. We analyze the thermal response for two distinct time periods: the forcing stage (0–3 days relative to storm passage) and the recovery stage (4–20 days relative to storm passage). This technique enables the characterization of the major sources of variability in the TC-induced ocean response, including cross-track variation, differences in storm intensity, and response time scale. We find this technique robustly captures the known characteristics of the vertical structure of the cross-track oceanic temperature response, and it provides a useful tool for examining basin-to-global representations of TC effects as a function of storm intensity.

Here we use the footprint method developed in part I to quantify OHC changes caused by TCs on a global scale. We focus on air–sea heat fluxes during storm passage and net ocean heat changes in the wakes of storms, relative to pre-storm conditions. The aim of the paper is to estimate observation-based OHC changes by TCs on basin and annual scales using vertically resolved Argo data and to explore implications for air–sea exchange and heat budgets. The paper is organized as follows. In Sect. 2, we present the method estimating the air–sea heat flux and ocean heat changes. We analyze the results of TC-induced air–sea heat fluxes in Sect. 3. In Sect. 4, we in-

calculated as follows (in W):

$$QA_{TSTD} =$$

$$L_{\text{track-TSTD}} \left[\int_{\text{dist}=-8}^{\text{dist}=8} \frac{1}{T_{3 \text{ days}}} \int_{\delta t=0}^{\delta t=3} \int_{\text{depth}=0}^{\text{depth}=1200} \rho c_p F_{TSTD}(\text{dist}, \text{depth}, \delta t) d_{\text{depth}} d_{\delta t} d_{\text{dist}} \right] / T_{\text{year}}$$

$$QA_{\text{Hur}} =$$

$$L_{\text{track-Hur}} \left[\int_{\text{dist}=-8}^{\text{dist}=8} \frac{1}{T_{3 \text{ days}}} \int_{\delta t=0}^{\delta t=3} \int_{\text{depth}=0}^{\text{depth}=1200} \rho c_p F_{\text{Hur}}(\text{dist}, \text{depth}, \delta t) d_{\text{depth}} d_{\delta t} d_{\text{dist}} \right] / T_{\text{year}}$$

where

F_{TSTD} , F_{Hur} – footprints of the track-averaged ocean responses obtained in part I of this study

c_p – heat capacity of sea water $\sim 4186 \text{ J}(\text{kg } ^\circ\text{C})^{-1}$

ρ – density of sea water, which are calculated by using Argo salinity, pressure and temperature measurements before the storm

δt – elapsed time after the storm passage, which is averaged from 0 to 3 days after storm passage

dist – cross-track distance from the location of the Argo pair to the track, which is set to 8° across the track

depth – vertical position of the measurement which is integrated from 0 to 1200 m

T_{year} – duration of one calendar year in seconds, to calculate an annual mean

$L_{\text{track-TSTD}}$, $L_{\text{track-Hur}}$ – averaged track length within one year, about $1.4 \times 10^8 \text{ m}$, $8.3 \times 10^7 \text{ m}$ for TS/TD and Hurricanes respectively, which are obtained by averaging the track length from 2004 to 2012.

We choose the time period between 0–3 days, because it likely captures the majority of the air–sea heat exchange during storm passage. However, other mechanisms may

Title Page

Abstract

Introduction

Conclusions

References

Tables

Figures

◀

▶

◀

▶

Back

Close

Full Screen / Esc

Printer-friendly Version

Interactive Discussion



Estimating air–sea heat fluxes and ocean heat content changes

L. Cheng et al.

Title Page

Abstract

Introduction

Conclusions

References

Tables

Figures

◀

▶

◀

▶

Back

Close

Full Screen / Esc

Printer-friendly Version

Interactive Discussion



also influence air–sea heat flux in this time period, such as storm induced cooling via mixing and wave generation. TC-induced surface cooling can cause a reversal of surface fluxes in the days following storm passage, which marks the transition between the forcing stage and the recovery stage. Some studies suggest fluxes may reverse sign around 2 days after TC passage (Dare and McBride, 2011; Lloyd and Vecchi, 2011), The exact timing of this reversal depends on many factors, such as storm intensity, translation speed and regional conditions, and the best choice is unclear in a global context. Thus, we use 3 days as conservative estimate. We performed sensitivity tests of the TC response to different choices of the time length (0–2, 0–2.5, 0–3.5 and 0–4 days), but the results (not shown), and the results and interpretations are generally consistent for all time scales.

2.2 Estimation of air–sea fluxes during TC passage

We examine the air–sea heat transfer rate in the TC-affected regions, by averaging air–sea heat flux as follows (in $W m^{-2}$):

$$H_{TSTD} = QA_{TSTD} / (L_{track-TSTD} \times R)$$

$$H_{Hur} = QA_{Hur} / (L_{track-Hur} \times R)$$

where R is the cross-track size of the TC-affected region which is set to be 16° ($\pm 8^\circ$ across the track). The other variables are consistent with QA_{TSTD} and QA_{Hur} .

2.3 Geographical distribution of air–sea heat fluxes

To calculate the geographical distribution of the TC-induced air–sea heat fluxes, we bin the global ocean using 1° by 1° grid boxes. From 2004 to 2012, the air–sea heat flux from each TC is calculated in each grid box (denoted as i and j for latitude and longitude respectively):

$$H_{i,j} = \left(\sum_{ID_1(i,j)}^{ID_2(i,j)} H_{TSTD} + \sum_{ID_1(i,j)}^{ID_2(i,j)} H_{Hur} \right) / T_{9\text{ years}}$$

where $T_{9\text{ years}}$ is the duration of 9 years in years. If a grid box is affected by two or more individual storms at the same time, only the heat flux due to the stronger storm is included. This avoids potential double-counting of storm effects. Annual air-sea heat flux is calculated by calculating the 9 year average (2004–2012). In this calculation, we assume that the heat exchange is uniform over the TC-affected region.

2.4 Estimation of net ocean heat content changes

We estimate the net OHC changes by examining the average temperature response between 4 to 20 after storm passage, referenced to pre-storm conditions. We choose 20 days as the maximum duration, because sea surface temperatures are typically restored by this time, and it is difficult to separate TC effects from seasonal signals on timescales greater than 3 weeks. Tests on the different choices of the time length are also conducted (4–18, 4–19 and 4–21 days). The results of these tests (not shown) suggest the magnitude of the TC signal is relatively insensitive to the choice of timescales.

We calculate OHC changes using (in W):

$$QN_{TSTD} = L_{\text{track-TSTD}} \left[\int_{\text{dist}=-8}^{\text{dist}=8} \frac{1}{T_{17\text{ days}}} \int_{\delta t=4}^{\delta t=20} \int_{\text{depth}=0}^{\text{depth}=1200} \rho c_p F_{TSTD}(\text{dist}, \text{depth}, \delta t) d_{\text{depth}} d_{\delta t} d_{\text{dist}} \right] / T_{\text{year}}$$

Estimating air–sea heat fluxes and ocean heat content changes

L. Cheng et al.

Title Page

Abstract

Introduction

Conclusions

References

Tables

Figures



Back

Close

Full Screen / Esc

Printer-friendly Version

Interactive Discussion



$QN_{Hur} =$

$$L_{\text{track-Hur}} \left[\int_{\text{dist}=-8}^{\text{dist}=8} \frac{1}{T_{17 \text{ days}}} \int_{\delta t=4}^{\delta t=20} \int_{\text{depth}=0}^{\text{depth}=1200} \rho c_p F_{\text{Hur}}(\text{dist}, \text{depth}, \delta t) d_{\text{depth}} d_{\delta t} d_{\text{dist}} \right] / T_{\text{year}}$$

where δt is the elapsed time after storm averaged from 4 to 20 days, $T_{17 \text{ days}}$ is the duration of 17 days in seconds. The other variables are the same to those in calculating QA_{TSTD} and QA_{Hur} .

2.5 Methodological limitations

Limitations of this methodology include:

1. To create the geographical distribution of air–sea heat fluxes, we assume that ocean response to a storm is the same everywhere (based on the composite analysis of the footprints). This assumption neglects the regional differences in the ocean response due to differences in the background state and seasonal effects.
2. The net OHC changes induced by TCs are averaged within 4–20 days after storm passage, which represents the restoration stage. However, the ocean changes may not be fully restored during this time interval. As noted previously, we choose this time period because TC signals are difficult to separate from the background seasonal cycle on longer time scales.
3. The internal waves generated by TCs induce fluctuations in temperature, which could potentially bias our results. However, we hypothesize that these wave effects average to zero because we are using a large number of Argo pairs (~ 4410). We discuss potential biases further in the following section.

3 Results and discussion

3.1 Estimate of air–sea heat flux

Here we calculate a global estimate of air–sea heat exchange during TCs by integrating the ocean heat differences within storm-affected regions during a 3 day interval surrounding storm passage. We assume that during this period, the net column-integrated ocean heat loss is caused by heat transfer from the ocean to the atmosphere. We use the footprint methodology described in part I, which has two spatial dimensions: vertical depth and cross-track distance relative to the storm’s direction of motion. The footprint averages over the along-track direction. Thus the footprint represents a 2-dimensional insulated box that is $\pm 8^\circ$ across the storm track relative to the storm center and 1200 m deep, with an opening at the air–sea interface. The heat exchange between the box and its surroundings occurs only at the surface.

To test whether assumptions about the footprint hold, particularly related to insulation from horizontal advection at the sides of the box and vertical heat exchange at the base, we calculate the box-averaged air–sea heat flux at different horizontal and vertical spatial scales, ranging from $dx = \pm 1$ to $\pm 15^\circ$ (with 0.5° increment) and $dz = 100$ to 1900 m (with 200 m increment). As shown in Fig. 1, the averaged air–sea heat flux stabilizes for $dx > \sim 6^\circ$. The decreasing trend for $dx > \sim 7^\circ$ is a “dilution” effect, which is caused by enlarging the box size while the OHC change within TC-affected region remains unchanged. Note this effect is generally linear for large dx , which is expected since the depth is held constant. In the vertical direction, the air–sea flux estimates are unchanged for dz greater than 700 m (corresponding to $dx > \sim 5^\circ$). This result suggests the method requires at least $\pm 7^\circ$ and 700 m in order for the insulated box assumption to be considered valid. Thus, we use a terminal depth $dz = 1200$ m based on the availability of data in the upper ocean (a large portion of Argos stop near 1200 m), and $dx = 8^\circ$.

The annual contribution of TCs to the air–sea heat fluxes for $dx = 8^\circ$ and $dz = 1200$ m is about ~ 4.80 and $\sim 6.25 \text{ W m}^{-2}$ for TS/TD and Hurricanes, respectively. The positive

Estimating air–sea heat fluxes and ocean heat content changes

L. Cheng et al.

Title Page

Abstract

Introduction

Conclusions

References

Tables

Figures



Back

Close

Full Screen / Esc

Printer-friendly Version

Interactive Discussion



Estimating air–sea heat fluxes and ocean heat content changes

L. Cheng et al.

Title Page

Abstract

Introduction

Conclusions

References

Tables

Figures

◀

▶

◀

▶

Back

Close

Full Screen / Esc

Printer-friendly Version

Interactive Discussion



activity, this peak is probably due to more TCs occurrences relative to other regions. In Fig. 4a and b, we present the frequency at each 1° by 1° grid box which is affected by TCs per year, given the affected regions (cross-track distance) defined to be ± 1 and $\pm 8^\circ$ relative to storm center. As expected, the figure shows a higher frequency of TC occurrences in grid boxes as we increase the size of the affected region. For example, in the western and eastern Pacific Ocean, between 1 and 1.5 storms pass directly through a single 1° by 1° grid box annually, but this activity can contribute to as much as 12 ~ 14 storms affecting the same grid boxes when we increase the TC-affected region to $\pm 8^\circ$.

To check whether the peak in heat flux is caused by increased frequency of TCs, we assume that one grid box can be affected by only one storm within 20 days. The annual air–sea heat fluxes for this method are presented in Fig. 5, showing the peak fluxes in the northwestern Pacific decrease to 30 W m^{-2} while the overall fluxes in the other basins are relatively unaffected (to within $\sim 5\text{--}10 \text{ W m}^{-2}$). Since the nature of air–sea heat exchanges is complicated by the close proximity of storms in active TC regions, such as in northwestern and northeastern Pacific, our geographical map of air–sea heat flux should be regarded as a first-order approximation.

3.2 Estimates of net OHC changes after storm

Net OHC changes are estimated by calculating the difference between the average post-storm temperature during wake recovery (between 4 and 20 days after storm passage) and the pre-storm conditions. We choose 20 days as the upper limit of the post-storm temperature, because it represents the time scale of SST recovery after storm passage. Temperature anomalies are plotted in Fig. 6 as a function of the spatial and vertical extents of the TC footprint. Within 3° of the storm center, both TS/TD and Hurricanes induce column-averaged cooling at all depths. The cooling effect decreases for increasing footprint size, approaching zero for TS/TD and a net warming for Hurricanes. This result suggests that upwelling and heat loss to the atmosphere near the storm center are partly (for TS/TD) or fully (for Hurricane) compensated by post-storm

during the recovery stage and thus net oceanic heat convergence. This finding is generally remarkably consistent with recent results analyzing satellite altimetry (Mei et al., 2013), who show positive oceanic heat convergence for hurricanes (~ 0.37 PW globally). And also this result is consistent with those presented in Srivier and Huber (2007) and Jansen et al. (2010).

It is important to note that this estimate averages the post-storm temperature between 4 and 20 days after storm passage. As a test of this assumption, we can also define the post-storm restoration period to be when the OHC change is to zero. In other words, post-storm warming balances the storm-induced enthalpy flux. Our estimates suggest that the OHC restoring period for hurricanes is less than 20 days but more than 20 days for TS/TD.

3.3 Uncertainties of the estimates

In the previous two sections, we estimate the annual air–sea heat fluxes during 0–3 days after storm passage and OHC changes during 4–20 days after storm passage relative to pre-storm conditions. Here we use a bootstrap technique to constrain the error bars and characterize the uncertainties of our heat flux and OHC estimates. Beginning with the total number of Argo float samples (4410 pairs), we randomly choose 90 % of pairs and repeat our air–sea heat flux and anomalous OHC calculations, as described in the previous sections. We repeat the calculation 200 times.

In Fig. 7b and d, 200 estimates of air–sea heat fluxes presented as function of horizontal footprint size of the TC-affected regions (distance to the storm center). Most of these bootstrap estimates exhibit similar patterns with those shown in Fig. 1, supporting the robustness of our estimates. We choose an error bar of one standard deviation near 8° to quantify the uncertainty of our estimate. This uncertainty measure is equal to $\pm 0.85 \text{ W m}^{-2}$ for TS/TD and $\pm 1.50 \text{ W m}^{-2}$ for Hurricanes, which is equivalent to ~ 20 and ~ 25 % of the fluxes for TS/TD and hurricanes, respectively. Or, in terms of global annual heat flux, this uncertainty equates to ± 0.20 PW for TS/TD and ± 0.21 PW for Hurricanes, which is equivalent to ~ 20 and ~ 25 % of the total estimates

Estimating air–sea heat fluxes and ocean heat content changes

L. Cheng et al.

Title Page

Abstract

Introduction

Conclusions

References

Tables

Figures



Back

Close

Full Screen / Esc

Printer-friendly Version

Interactive Discussion



for TS/TD and Hurricanes, respectively. Including these uncertainties, our estimates of air–sea heat flux during the TC forcing stage (0–3 days relative to storm passage) are: 1.05 ± 0.20 PW (4.8 ± 0.85 W m⁻²) for TS/TD and 0.82 ± 0.21 PW (6.25 ± 1.5 W m⁻²) for hurricanes.

Similarly, the 200 estimates of TC-induced OHC changes are shown in Fig. 8. We choose the uncertainty to be equivalent to the standard deviation of the average temperature change for spatial extent of 8° and 1200 m, consistent with the heat flux estimate. This uncertainty equates to ± 0.0063 °C for TS/TD and ± 0.0143 °C for hurricanes, which represents ~ 50 and 36 % of the estimated OHC changes for TS/TD and hurricanes, respectively. Considering this uncertainty, our estimates of TC-induced thermal changes are: -0.0125 ± 0.0063 °C for TS/TD and 0.0390 ± 0.0143 °C for hurricanes. Equivalently, these estimates correspond to global annual heat flux of -0.41 ± 0.21 PW (-1.90 ± 0.96 W m⁻²) for all TS/TDs, and 0.75 ± 0.25 PW (5.98 ± 2.1 W m⁻²) for all hurricanes, where the positive values denote a net oceanic heat convergence.

4 Conclusion and discussion

We examine TCs' contribution to global annual air–sea heat flux and net OHC changes by using the ARGO observing system. We find that during the storm passage, the ocean generally experiences a net heat loss to the atmosphere through storm-induced enthalpy fluxes. Our observational results suggest that TCs contribute 11.5 W m⁻² (1.87 PW) heat in TC-affected regions annually from the ocean to the atmosphere within 0–3 days after storm passage. Of this total, weak storm (TS/TD) contribute 4.80 W m⁻² (1.05 PW) and strong storms (hurricanes) account for the rest. The uncertainty of our estimate is about 20 % for TS/TD and 25 % for hurricanes.

Recent in-situ, remotely sensed and reanalyzed air–sea heat flux products (Smith et al., 2011) have faced challenges in closing the ocean heat budget. These analyses show a net global oceanic heat gain of 20–30 W m⁻² (Josey et al., 1999), while the global mean net heat flux is ~ 0.5 W m⁻² from observed variations in OHC. Our obser-

Estimating air–sea heat fluxes and ocean heat content changes

L. Cheng et al.

Title Page

Abstract

Introduction

Conclusions

References

Tables

Figures

◀

▶

◀

▶

Back

Close

Full Screen / Esc

Printer-friendly Version

Interactive Discussion



vational results suggest that TCs may provide a potential mechanism (heat flux in high wind regime) for filling this gap.

After storm passage, ocean conditions in TC-affected regions experience a recovery process to at least partially restore upper ocean conditions pre-storm or climatological values through enhanced air–sea fluxes leading to ocean heat convergence. This recovery stage lasts much longer than the forcing stage during the storm passage. We estimate the net changes in a time scale of 4–20 days relative to pre-storm conditions, which implicitly includes fluxes during the forced stage. On this time scale, around ~ 0.75 PW (5.98 W m^{-2}) of heat is transferred annually from atmosphere to the ocean for hurricanes, which represents a net ocean heat gain after storms. However, TS/TD exhibit an opposite response, ~ -0.41 PW (1.90 W m^{-2}), representing a net ocean heat loss for weaker events. We estimate the uncertainty to be about 50 % of our estimates for TS/TD and 35 % for Hurricanes. The opposite sign of net OHC changes after storm (4–20 days) for weak and strong storms implies the impact of these events on the upper ocean is sensitive to the intensity. This result also suggests that additional atmospheric heating due to anthropogenic warming may potentially increase the rate of TC-induced ocean heat uptake, since research suggests the number of strong TCs may increase with continued warming (Bender et al., 2010; Knutson et al., 2010).

To assess the TC contribution to historical trends in the ocean heat uptake, we calculate the total air–sea heat flux in each year from 1970 to 2010, by assuming that each TS/TD transfers 6.25 W m^{-2} and each hurricane transfers 4.8 W m^{-2} heat from the TC-affected region to the atmosphere during 0–3 days after storm. The annual heat flux is shown in Fig. 9 in blue. The figure shows a maximum atmospheric heating $\sim 12 \times 10^{22}$ J during 1996–1997 and a generally larger signal between 1988 and 1998, which is due to more TC activity during these years. As suggested in Trenberth and Fasullo, (2007), the large El Nino activity during these years (3 between 1990–1995 and a large event in 1997–1998) may be at least partially responsible this boost in activity in key TC regions (e.g. west Pacific).

Estimating air–sea heat fluxes and ocean heat content changes

L. Cheng et al.

Title Page

Abstract

Introduction

Conclusions

References

Tables

Figures



Back

Close

Full Screen / Esc

Printer-friendly Version

Interactive Discussion



References

- Bell, M. M., Montgomery, M. T., and Emanuel, K. A.: Air–sea enthalpy and momentum exchange at major hurricane wind speeds observed during CBLAST, *J. Atmos. Sci.*, 69, 3197–3222, doi:10.1175/jas-d-11-0276.1, 2012.
- 5 Bender, M. A., Knutson, T. R., Tuleya, R. E., Sirutis, J. J., Vecchi, G. A., Garner, S. T., and Held, I. M.: Modeled impact of anthropogenic warming on the frequency of intense Atlantic hurricanes, *Science*, 327, 454–458, doi:10.1126/science.1180568, 2010.
- Black, W. J. and Dickey, T. D.: Observations and analyses of upper ocean responses to tropical storms and hurricanes in the vicinity of Bermuda, *J. Geophys. Res.-Oceans*, 113, C08009, doi:10.1029/2007JC004358, 2008.
- 10 Braun, S. A.: High-resolution simulation of Hurricane Bonnie, 1998. Part II: Water budget, *J. Atmos. Sci.*, 63, 43–64, 2006.
- Cheng, L. and Zhu, J.: Artifacts in variations of ocean heat content induced by the observation system changes, *Geophys. Res. Lett.*, 41, 7276–7283, doi:10.1002/2014GL061881, 2014.
- 15 D’Asaro, E. A.: The ocean boundary layer below Hurricane Dennis, *J. Phys. Oceanogr.*, 33, 561–579, 2003.
- Dare, R. A. and McBride, J. L.: Sea surface temperature response to tropical cyclones, *Mon. Weather Rev.*, 139, 3798–3808, 2011.
- Domingues, C. M., Church, J. A., White, N. J., Gleckler, P. J., Wijffels, S. E., Barker, P. M., and 20 Dunn, J. R.: Improved estimates of upper-ocean warming and multi-decadal sea-level rise, *Nature*, 453, 1090–1096, 2008.
- Emanuel, K.: Environmental factors affecting tropical cyclone power dissipation, *J. Climate*, 20, 5497–5509, doi:10.1175/2007jcli1571.1, 2007.
- Emanuel, K. A.: The theory of hurricanes, *Annu. Rev. Fluid Mech.*, 23, 179–196, 1991.
- 25 Emanuel, K. A.: Thermodynamic control of hurricane intensity, *Nature*, 401, 665–669, 1999.
- Fedorov, A. V., Brierley, C. M., and Emanuel, K.: Tropical cyclones and permanent El Niño in the early Pliocene epoch, *Nature*, 463, 1066–1084, doi:10.1038/Nature08831, 2010.
- Ginis, I.: Interaction of tropical cyclones with the ocean, in: *Global Perspective of Tropical Cyclones*, Chapter 5, edited by: Elsberry, R. L., Tech. Document WMO/TD 693, World Meteorological Organization, Geneva, Switzerland, 198–260, 1995.
- 30 Jansen, M. F., Ferrari, R., and Mooring, T. A.: Seasonal vs. permanent thermocline warming by tropical cyclones, *Geophys. Res. Lett.*, 37, L03602, doi:10.1029/2009gl041808, 2010.

Estimating air–sea heat fluxes and ocean heat content changes

L. Cheng et al.

Title Page

Abstract

Introduction

Conclusions

References

Tables

Figures



Back

Close

Full Screen / Esc

Printer-friendly Version

Interactive Discussion



Estimating air–sea heat fluxes and ocean heat content changes

L. Cheng et al.

Title Page

Abstract

Introduction

Conclusions

References

Tables

Figures

◀

▶

◀

▶

Back

Close

Full Screen / Esc

Printer-friendly Version

Interactive Discussion



- Josey, S. A., Kent, E. C., and Taylor, P. K.: New insights into the ocean heat budget closure problem from analysis of the SOC air–sea flux climatology, *J. Climate*, 12, 2856–2880, 1999.
- Kalnay, E., Kanamitsu, M., Kistler, R., Collins, W., Deaven, D., Gandin, L., Iredell, M., Saha, S., White, G., Woollen, J., Zhu, Y., Leetmaa, A., and Reynolds, R.: The NCEP/NCAR 40 year reanalysis project, *B. Am. Meteorol. Soc.*, 77, 437–471, 1996.
- Knutson, T. R., McBride, J. L., Chan, J., Emanuel, K., Holland, G., Landsea, C., Held, I., Kossin, J. P., Srivastava, A. K., and Sugi, M.: Tropical cyclones and climate change, *Nat. Geosci.*, 3, 157–163, 2010.
- Levitus, S., Antonov, J. I., Boyer, T. P., Locarnini, R. A., Garcia, H. E., and Mishonov, A. V.: Global ocean heat content 1955–2008 in light of recently revealed instrumentation problems, *Geophys. Res. Lett.*, 36, L07608, doi:10.1029/2008GL037155, 2009.
- Levitus, S., Antonov, J. I., Boyer, T. P., Baranova, O. K., Garcia, H. E., Locarnini, R. A., Mishonov, A. V., Reagan, J. R., Seidov, D., Yarosh, E. S., and Zweng, M. M.: World ocean heat content and thermosteric sea level change, 0–2000 m: 1955–2010, *Geophys. Res. Lett.*, 39, L10603, doi:10.1029/2012GL051106, 2012.
- Lin, I. I., Chen, C. H., Pun, I. F., Liu, W. T., and Wu, C. C.: Warm ocean anomaly, air sea fluxes, and the rapid intensification of tropical cyclone Nargis, 2008, *Geophys. Res. Lett.*, 36, L03817, doi:10.1029/2008GL035815, 2009.
- Lloyd, I. D. and Vecchi, G. A.: Observational evidence for oceanic controls on hurricane intensity, *J. Climate*, 24, 1138–1153, 2011.
- Mcphaden, J. M., Foltz, G. R., Lee, T., Murty, V. S. N., Ravichandran, M., Vecchi, G. A., Vialard, J., Wiggert, J. D., and Yu, L.: Ocean–atmosphere interactions during cyclone Nargis, *EOS T. Am. Geophys. Un.*, 90, 53–54, doi:10.1029/2009EO070001, 2009.
- Mei, W., Primeau, F., McWilliams, J. C., and Pasquero, C.: Sea surface height evidence for long-term warming effects of tropical cyclones on the ocean, *P. Natl. Acad. Sci. USA*, 110, 15207–15210, 2013.
- Park, J. J., Kwon, Y. O., and Price, J. F.: Argo array observation of ocean heat content changes induced by tropical cyclones in the north Pacific, *J. Geophys. Res.*, 116, C12025, doi:10.1029/2011JC007165, 2011.
- Powell, M. D., Vickery, P. J., and Reinhold, T. A.: Reduced drag coefficient for high wind speeds in tropical cyclones, *Nature*, 422, 279–283, 2003.
- Price, J. F.: Upper ocean response to a hurricane, *J. Phys. Oceanogr.*, 11, 153–175, 1981.

Estimating air–sea heat fluxes and ocean heat content changes

L. Cheng et al.

Title Page

Abstract

Introduction

Conclusions

References

Tables

Figures



Back

Close

Full Screen / Esc

Printer-friendly Version

Interactive Discussion



Price, J. F.: Internal wave wake of a moving storm. 1. Scales, energy budget and observations, *J. Phys. Oceanogr.*, 13, 949–965, 1983.

Smith, S. R., Hughes, P. J., and Bourassa, M. A.: A comparison of nine monthly air–sea flux products, *Int. J. Climatol.*, 31, 1002–1027, doi:10.1002/joc.2225, 2011.

5 Sriver, R. L. and Huber, M.: Observational evidence for an ocean heat pump induced by tropical cyclones, *Nature*, 447, 577–580, doi:10.1038/Nature05785, 2007.

Sriver, R. L., Huber, M., and Nusbaumer, J.: Investigating tropical cyclone-climate feedbacks using the TRMM Microwave Imager and the Quick Scatterometer, *Geochem. Geophys. Geosy.*, 9, Q09V11, doi:10.1029/2007gc001842, 2008.

10 Sriver, R. L., Goes, M., Mann, M. E., and Keller, K.: Climate response to tropical cyclone-induced ocean mixing in an Earth system model of intermediate complexity, *J. Geophys. Res.-Oceans*, 115, C10042, doi:10.1029/2010jc006106, 2010.

Trenberth, K. E. and Fasullo, J.: Water and energy budgets of hurricanes and implications for climate change, *J. Geophys. Res.-Atmos.*, 112, D23107, doi:10.1029/2006JD008304, 2007.

15 Trenberth, K. E., Davis, C. A., and Fasullo, J.: Water and energy budgets of hurricanes: case studies of Ivan and Katrina, *J. Geophys. Res.-Atmos.*, 112, D23106, doi:10.1029/2006JD008303, 2007.

Trenberth, K. E., Fasullo, J. T., and Kiehl, J.: Earth's global energy budget, *B. Am. Meteorol. Soc.*, 90, 311–323, doi:10.1175/2008BAMS2634.1, 2009.

20 von Schuckmann, K. and Le Traon, P.-Y.: How well can we derive Global Ocean Indicators from Argo data?, *Ocean Sci.*, 7, 783–791, doi:10.5194/os-7-783-2011, 2011.

Willis, J. K., Chambers, D. P., and Nerem, R. S.: Assessing the globally averaged sea level budget on seasonal to interannual timescales, *J. Geophys. Res.-Oceans*, 113, C06015, doi:10.1029/2007JC004517, 2008.

25 Wright, C. W., Walsh, E. J., Vandemark, D., Krabill, W. B., Garcia, A. W., Houston, S. H., Powell, M. D., Black, P. G., and Marks, F. D.: Hurricane directional wave spectrum spatial variation in the open ocean, *J. Phys. Oceanogr.*, 31, 2472–2488, 2001.

Estimating air–sea heat fluxes and ocean heat content changes

L. Cheng et al.

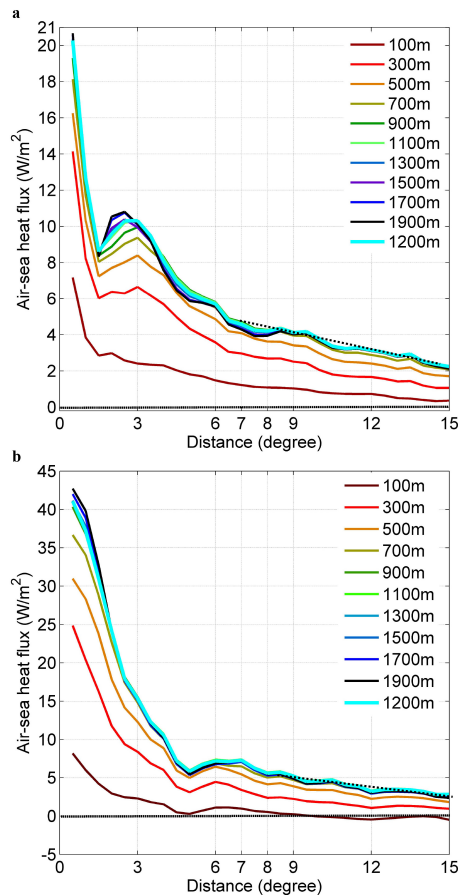


Figure 1. Estimates of air–sea heat flux within TC with different footprint domain sizes (horizontal and depth) for: **(a)** TS/TDs and **(b)** hurricanes. The results of 1200 m are highlighted in cyan.

[Title Page](#)
[Abstract](#)
[Introduction](#)
[Conclusions](#)
[References](#)
[Tables](#)
[Figures](#)
[◀](#)
[▶](#)
[◀](#)
[▶](#)
[Back](#)
[Close](#)
[Full Screen / Esc](#)
[Printer-friendly Version](#)
[Interactive Discussion](#)


Estimating air–sea heat fluxes and ocean heat content changes

L. Cheng et al.

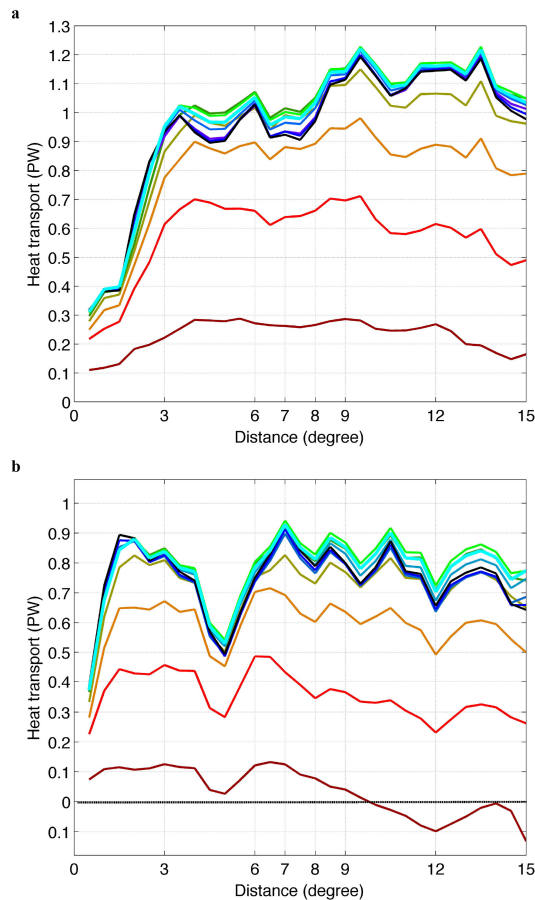


Figure 2. The impacts of domain size on global annual heat transfer from the ocean to the atmosphere by TCs for: **(a)** TS/TDs and **(b)** hurricanes. The colors are the same to those in Fig. 1.

[Title Page](#)[Abstract](#)[Introduction](#)[Conclusions](#)[References](#)[Tables](#)[Figures](#)[◀](#)[▶](#)[◀](#)[▶](#)[Back](#)[Close](#)[Full Screen / Esc](#)[Printer-friendly Version](#)[Interactive Discussion](#)

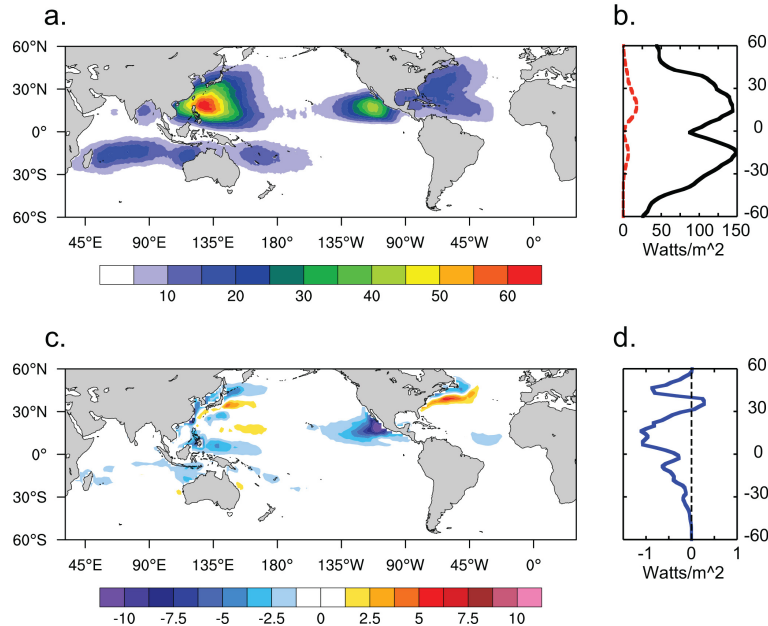


Figure 3. Geographical pattern of air–sea heat flux caused by TCs. **(a)** Globally integrated net heat flux caused by TCs calculated using Argo float data ($W m^{-2}$). **(b)** Zonally averaged TC-induced heat flux (red curve), compared with the annual climatology (1990–2010) of air–sea latent heat flux (black curve) derived from NCEP/NCAR reanalysis (Kalnay et al., 1996). **(c)** Net surface flux (positive upward) along storm tracks for climatological conditions during the period 1990–2010 ($W m^{-2}$), derived from NCEP/NCAR reanalysis using storm tracks from 1990–2010. The plot represents the background air–sea flux contribution to the Argo analysis using the 20 year daily climatology. **(d)** Zonal average of the climatological net surface heat fluxes shown in c.

Estimating air–sea heat fluxes and ocean heat content changes

L. Cheng et al.

Title Page

Abstract Introduction

Conclusions References

Tables Figures

◀ ▶

◀ ▶

Back Close

Full Screen / Esc

Printer-friendly Version

Interactive Discussion



Estimating air–sea heat fluxes and ocean heat content changes

L. Cheng et al.

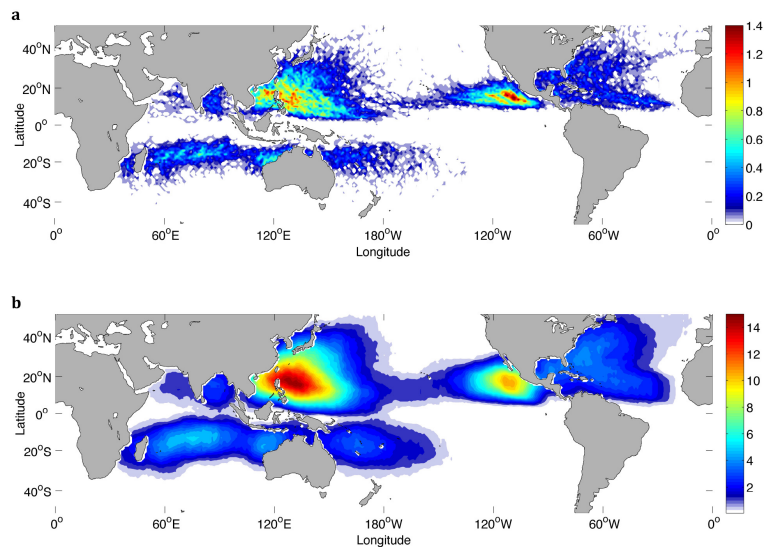


Figure 4. Frequencies of tropical cyclones per year affecting 1° by 1° grid boxes, when the TC-affected region is assumed to be **(a)** $\pm 1^\circ$ from the track center, and **(b)** $\pm 8^\circ$ from the track center.

[Title Page](#)[Abstract](#)[Introduction](#)[Conclusions](#)[References](#)[Tables](#)[Figures](#)[◀](#)[▶](#)[◀](#)[▶](#)[Back](#)[Close](#)[Full Screen / Esc](#)[Printer-friendly Version](#)[Interactive Discussion](#)

Estimating air–sea heat fluxes and ocean heat content changes

L. Cheng et al.

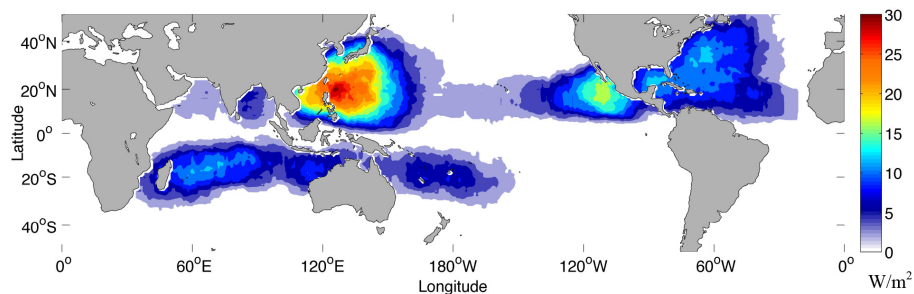


Figure 5. Geographical distribution of air–sea heat flux caused by TCs. We assume each grid box can only be affected by 1 storm within a 20 day window.

[Title Page](#)[Abstract](#)[Introduction](#)[Conclusions](#)[References](#)[Tables](#)[Figures](#)[◀](#)[▶](#)[◀](#)[▶](#)[Back](#)[Close](#)[Full Screen / Esc](#)[Printer-friendly Version](#)[Interactive Discussion](#)

Estimating air–sea heat fluxes and ocean heat content changes

L. Cheng et al.

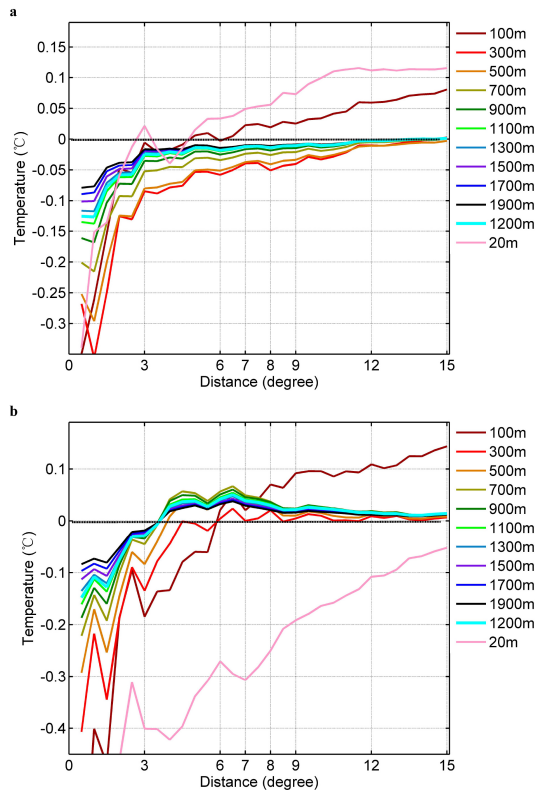


Figure 6. Column averaged temperature anomalies within 4–20 days after tropical cyclones, relative to pre-storm conditions, as a function of the horizontal box size across the storm track (from ± 1 to $\pm 15^\circ$) for: **(a)** TS/TD, and **(b)** hurricanes. The colors are different vertical size of the TC-affected box from 100 to 1900 m. The results for the box with 1200 m depth is highlighted in cyan.

[Title Page](#)
[Abstract](#)
[Introduction](#)
[Conclusions](#)
[References](#)
[Tables](#)
[Figures](#)
[◀](#)
[▶](#)
[◀](#)
[▶](#)
[Back](#)
[Close](#)
[Full Screen / Esc](#)
[Printer-friendly Version](#)
[Interactive Discussion](#)


Estimating air–sea heat fluxes and ocean heat content changes

L. Cheng et al.

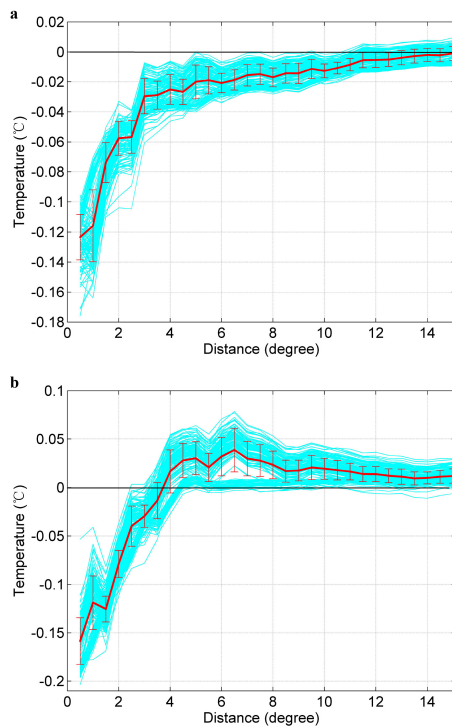


Figure 8. 200 estimates (in cyan) of 0–1200 m column averaged temperature as a function of distance across the storm track, based on randomly sampling 90% of the Argo pairs for: **(a)** TS/TD and **(b)** hurricanes respectively. The mean and standard deviations are highlighted as the red line and error bars.

[Title Page](#)[Abstract](#)[Introduction](#)[Conclusions](#)[References](#)[Tables](#)[Figures](#)[◀](#)[▶](#)[◀](#)[▶](#)[Back](#)[Close](#)[Full Screen / Esc](#)[Printer-friendly Version](#)[Interactive Discussion](#)

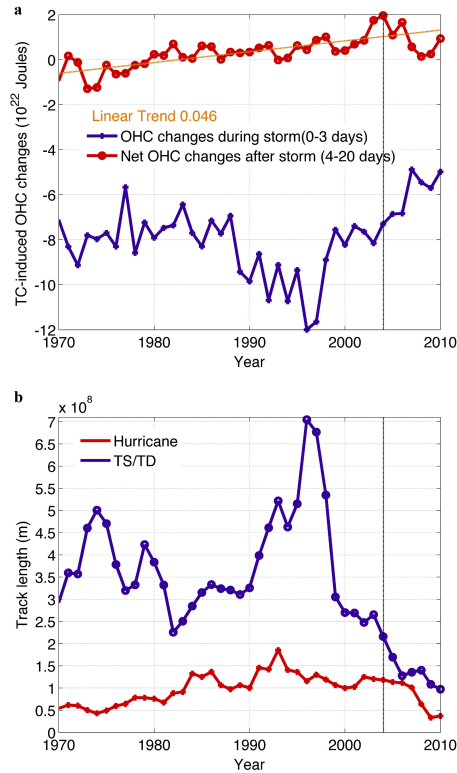


Figure 9. (a) The annual TC-induced ocean heat loss via air–sea heat flux in 0–3 days (blue line) and the net ocean heat content changes after storm (in 4–20 days) (red line). The positive values show the net heat gain. The linear trend of the net ocean heat gain is presented in pink, and the trend is $0.046 \times 10^{22} \text{ J year}^{-1}$. (b) Yearly averaged track lengths for both TS/TD (blue) and hurricanes (in red).